Engineering 3 (2017) 365–378

Contents lists available at ScienceDirect

Engineering

journal homepage: www.elsevier.com/locate/eng

Research
Green Chemical Engineering—Review

Tantalum (Oxy)Nitride: Narrow Bandgap Photocatalysts for Solar Hydrogen Generation

Mu Xiao, Songcan Wang, Supphasin Thaweesak, Bin Luo, Lianzhou Wang*

Nanomaterials Center, School of Chemical Engineering, and Australian Institute for Bioengineering and Nanotechnology, The University of Queensland, Brisbane, QLD 4072, Australia

ARTICLE INFO

Article history:
Received 15 February 2017
Revised 4 May 2017
Accepted 5 May 2017
Available online 22 May 2017

Keywords:
Tantalum-based photocatalyst
Narrow bandgap
Water splitting
Hydrogen

ABSTRACT

Photocatalytic water splitting, which directly converts solar energy into hydrogen, is one of the most desirable solar-energy-conversion approaches. The ultimate target of photocatalysis is to explore efficient and stable photocatalysts for solar water splitting. Tantalum (oxy)nitride-based materials are a class of the most promising photocatalysts for solar water splitting because of their narrow bandgaps and sufficient band energy potentials for water splitting. Tantalum (oxy)nitride-based photocatalysts have experienced intensive exploration, and encouraging progress has been achieved over the past years. However, the solar-to-hydrogen (STH) conversion efficiency is still very far from its theoretical value. The question of how to better design these materials in order to further improve their water-splitting capability is of interest and importance. This review summarizes the development of tantalum (oxy)nitride-based photocatalysts for solar water spitting. Special interest is paid to important strategies for improving photocatalytic water-splitting efficiency. This paper also proposes future trends to explore in the research area of tantalum-based narrow bandgap photocatalysts for solar water splitting.

1. Introduction

Considering environmental problems and the exhausting supply of global energy, it is urgently necessary to exploit sustainable energy systems. Solar energy, as a clean, renewable, and abundant energy, is one of the most promising candidates to substitute for fossil fuels. With a specific energy density of 120 $kJ \cdot g^{-1}$ and only water (H_2O) as a byproduct when consumed, hydrogen (H_2) is considered to be an efficient energy carrier as well as the cleanest option [1–3]. Moreover, H_2 can be stored and carried over a long distance as a stable energy supply [2–4]. Photocatalytic water splitting, which stores solar energy in H—H (H_2) bonds, is a simple and green solar-energy-conversion approach [1], and has therefore attracted global research interest during the past decades. Many materials have been investigated for solar water splitting with the hope of achieving a commercially feasible solar-to-hydrogen (STH) efficiency of over 10% [5–10]. To date, some material systems can achieve overall water splitting, but most of these photocatalysts can only be active under ultraviolet (UV) light irradiation (which accounts for only 4% of solar energy) [11–14]. Only limited material systems, such as $In_{1-x}Ni_xTaO_4$ (x = 0–0.2) [15], $(Ga_{1-x}Zn_x)(N_{1-x}O_x)$ [16], $(Zn_{1+x}Ge)(N_2O_x)$ [17], TaON [18], C_3N_4 [19,20], and $LaMg_xTa_{1-x}O_{1+3x}N_{2-3x}$ (x = 0–2/3) [21], are able to achieve visible-light-responsible water splitting. However, the STH efficiency of these photocatalysts is still too low for practical application. Many metal dichalcogenides (e.g., CdS, CdSe, and $CuInS_2$), which can absorb visible light, show highly efficient photocatalytic H_2 evolution from water with sacrificial agents [22–24]. However, most suffer from photocorrosion, which damages the long-term stability of these photocatalysts. Therefore, the question of how to better design and develop low-cost and stable photocatalysts for efficient water splitting is of great importance.

As many excellent reviews for photocatalytic water splitting have

* Corresponding author.
E-mail address: l.wang@uq.edu.au

http://dx.doi.org/10.1016/J.ENG.2017.03.019

been published [6,7,11,12,25–35], we provide only a brief introduction to the photocatalytic water-splitting mechanism here. As shown in Fig. 1, the major steps in a photocatalytic water-splitting reaction are as follows.

(1) Photon absorption and electron-hole pair generation. During this process, only photons with energy higher than the bandgap energy of the semiconductor are effective for excitation. Once excited, electrons from valence bands (VBs) jump to conduction bands (CBs), and holes are left in the VBs. The photo-excited electrons and holes lead to redox reactions on H_2O, electrons for water reduction, and holes for water oxidation. As illustrated in Fig. 2, the energy potential of the CB minimum and VB maximum are key points for the photocatalytic reaction. The CB minimum should be more negative than the H_2 production potential (0 V vs. normal hydrogen electrode (NHE) while the VB maximum should be more positive than the oxygen production potential (1.23 V). Otherwise, the photocatalysts can only conduct a half reaction with the assistance of sacrificial agents, which will increase the cost of the hydrogen produced.

(2) Separation and transfer of electrons. Photo-generated electron-hole pairs separate and migrate to the surface to take part in the water redox reaction. During this process, charge carriers easily meet each other and recombination occurs, which is undesirable for photocatalysis.

(3) Surface chemical reactions. In this step, the photo-excited charge carriers on the surface active sites react with water.

Due to the 10% STH conversion efficiency that is required for commercial application, the development of highly efficient photocatalysts that can maximize the efficiency of each of the three steps mentioned above is extremely important [1,36–38]. The theoretical maximum STH efficiency depends on the bandgap of the photocatalysts, because only light with energy higher than the bandgap of the photocatalysts can be absorbed and used for the water redox reaction. Theoretically, the bandgap should be a minimum of 1.23 eV. However, due to the thermodynamic energy (~0.4 eV) and kinetic loss (~0.4 eV), a bandgap of 2 eV is usually necessary for overall photocatalytic water splitting [11]. For photocatalysts with a bandgap energy ranging from 2.0 eV to 2.5 eV, the theoretical STH efficiency ranges from 10% to 16% under simulated sunlight irradiation (air mass 1.5 global, AM 1.5G) [39]. Considering the energy loss in practical applications, a narrow bandgap is a key criterion for photocatalysts to achieve high STH efficiency. Here, we define narrow bandgap photocatalysts as photocatalysts with a bandgap no greater than 2.5 eV (corresponding to ~500 nm light absorption).

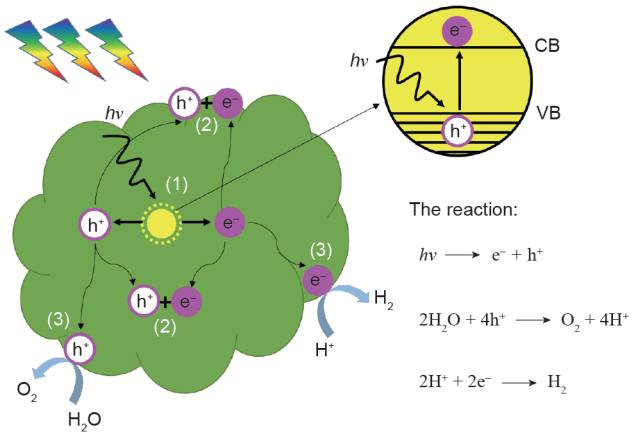

Fig. 1. Main scheme of photocatalytic water splitting. CB: conduction band; VB: valence band.

Tantalum (oxy)nitride-based photocatalysts, which have bandgaps varying from 1.9 eV to 2.5 eV and bandgap positions that are suitable for water splitting, are considered to be a group of potential photocatalysts for efficient water splitting [39]. Over the past years, great development and encouraging progress have been achieved in tantalum (oxy)nitride-based photocatalysts. However, the STH efficiency of these photocatalysts is still less than 1% [40–45]. One major problem is the asymmetric capability of these materials for water reduction and oxidation. Tantalum (oxy)nitride-based photocatalysts have shown a comparably much higher water oxidation capability than water reduction capability [40,46–48]. Because overall water splitting is a synergistic reaction system between water reduction and water oxidation, a relatively weaker water reduction capability will inevitably impede the overall water-splitting reaction. Thus, it is of great importance to improve the water reduction efficiency of tantalum (oxy)nitride-based photocatalysts. In addition, both surface defects and self-oxidation damage the long-term stability of tantalum (oxy)nitride-based photocatalysts. This review provides an up-to-date critical review on narrow bandgap tantalum (oxy)nitride-based photocatalysts for water splitting. In particular, recent progress in the development of effective strategies for enhancing their water reduction capability is discussed. An outlook perspective for further development of tantalum (oxy)nitride-based photocatalysts is also proposed.

2. Tantalum-based narrow bandgap photocatalysts

Tantalum (oxy)nitride-based photocatalysts are a large family; the main research focus is on Ta_3N_5, TaON, $LaTaON_2$, and $ATaO_2N$ (A = Ca, Sr, Ba), which possess narrow bandgaps and suitable band positions for the water redox reaction [49]. Among these, Ta_3N_5 and TaON have been intensely studied, and over 10% quantum efficiency (QE) for water oxidation and 9.5% QE for water reduction

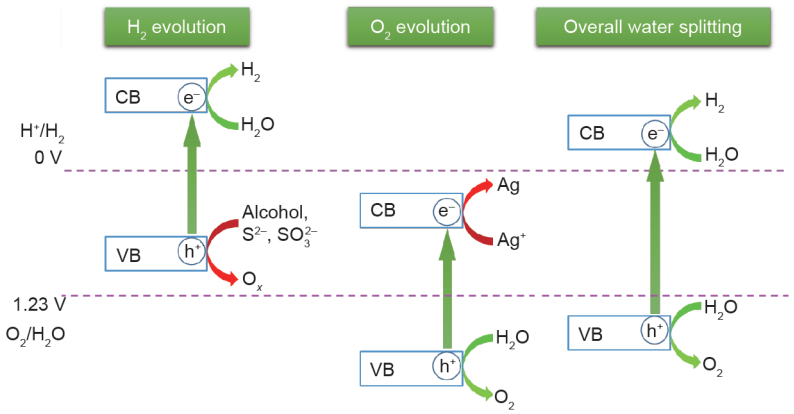

Fig. 2. Scheme of water splitting using semiconductors.

have been achieved [43,47,48]. In addition, $BaTaO_2N$ has shown H_2 evolution from water without sacrificial agents by forming a solid solution with $BaZrO_3$, and TaON was demonstrated to show overall water-splitting activity with surface modification and appropriate co-catalysts [18,50]. Moreover, very recent progress showed that $LaMg_xTa_{1-x}O_{1+3x}N_{2-3x}$ and $CaTaO_2N$ could achieve overall water splitting when a Rh-Cr bimetallic oxide co-catalyst was loaded on the surface [51]. All these findings strongly indicate the great potential of tantalum (oxy)nitride-based narrow bandgap photocatalysts for achieving highly efficient solar water splitting.

2.1. Basic properties of tantalum (oxy)nitrides

Many reviews have introduced and discussed the fundamental parameters, optical properties, and electronic properties of tantalum (oxy)nitride-based materials, both theoretically and experimentally [14,30,41,42,52,53]. Here, we briefly introduce the basic properties that are relevant to photocatalytic performance. Table 1 [49] presents typical tantalum (oxy)nitride-based photocatalysts. Ta_3N_5 and TaON show anosovite- and baddelyite-type crystal structures, respectively, while the others are perovskite-type crystals. The bandgap ranges from 1.9 eV to 2.4 eV, and corresponds to as long as 660 nm light absorption. The absolute position of the CB minimum and of the VB maximum is one of the key factors that influences the water reduction and water oxidation capability of photocatalysts. Domen et al. [54] experimentally identified the CB and VB positions of Ta_3N_5 and TaON by combining UV photoelectron spectroscopy (UPS) with electrochemical analysis. As shown in Fig. 3 [54], the CB minimums of Ta_3N_5 and TaON are ~−0.3 eV and ~−0.5 eV, respectively, versus NHE at pH = 0, while the VB maximums of Ta_3N_5 and TaON are ~1.6 eV and ~2.1 eV, respectively. The bandgap positions indicate that both Ta_3N_5 and TaON can be used for the photocatalytic water redox reaction. Balaz et al. [55] investigated the bandgap positions of tantalum oxynitride perovskite ($ATaO_2N$, A = Ca, Sr, Ba) by combining depth-resolve cathodoluminescence spectroscopy (DRCLS), ultraviolet-visible (UV-Vis) spectroscopy, Kelvin probe force microscopy (KPFM), and X-ray photoemission spectroscopy (XPS). As shown in Fig. 4 [55], all of the VB maximums except that of $PrTaO_2N$ are more positive than the oxygen evolution potential of water, and the CB minimums are more negative than the hydrogen evolution potential. Based on the investigation of band structure and the study of photocatalytic water-splitting activity, it is anticipated that tantalum (oxy)nitride-based materials can be designed as highly efficient catalysts for solar water splitting.

Table 1
Representative tantalum (oxy)nitride-based photocatalysts [49].

Compound	Crystal structure	Absorption edge (nm)	Bandgap (eV)
Ta_3N_5	Anosovite	600	2.1
TaON	Baddelyite	510	2.4
$LaTaON_2$	Perovskite	640	1.9
$CaTaO_2N$	Perovskite	510	2.4
$SrTaO_2N$	Perovskite	570	2.2
$BaTaO_2N$	Perovskite	660	1.9

2.2. Synthesis of tantalum (oxy)nitrides

In general, tantalum (oxy)nitride-based materials are synthesized from tantalum-based oxide precursors via nitridation at high temperature with ammonia (NH_3) gas as the nitrogen source [14]. For Ta_3N_5 and TaON, many preparation methods have been reported to synthesize Ta_2O_5 precursors, including reverse homogeneous precipitation reactive sputtering, atomic layer deposition, and vapor phase hydrothermal processes [56–61]. For the tantalum-based oxynitride perovskite, a solid-state reaction is normally applied to synthesize the oxide precursors. The key step to transform the precursors into (oxy)nitride is high-temperature thermal treatment in NH_3 gas. The nitridation conditions, such as temperature, pressure, and precursor, are important to the final photocatalytic performance [62–64].

The nitridation temperature, duration, and NH_3 gas flow determine the final products. During the nitridation process, the oxygen (O) atoms are substituted by nitrogen (N) atoms. When using Ta_2O_5 as the precursor, low temperature, short time, and low NH_3 gas flow lead to a slow reaction and to the partial substitution of O atoms by N atoms, resulting in TaON as the final product. To obtain oxygen-free Ta_3N_5, higher temperature (> 850 °C), longer treatment (> 10 h), and higher NH_3 gas flow (> 20 mL·min^{-1}) are necessary. The influence of nitridation temperature on the photocatalytic performance of Ta_3N_5 has been systematically studied [62]. During the nitridation process, the duration and NH_3 gas flow were fixed, with the only variation being that of temperature. Once the temperature was above 850 °C, Ta_3N_5 could be obtained. Further increasing the temperature to 950 °C did not influence the structural and optical properties of Ta_3N_5. However, increasing the temperature to 1000 °C led to the formation of a tantalum (Ta) reduced species, which was confirmed by the sub-bandgap absorption that was observed in the UV-Vis light absorption spectrum (Fig. 5) [62]. The Ta reduced species acted as a recombination center, and samples with such defects showed lower photocatalytic performance. Thus, suitable nitridation temperature is important to obtain Ta_3N_5 with good crystallinity and pure phase.

Pressure is another factor that influences the final performance of tantalum (oxy)nitride photocatalysts [65]. Kishida and Watanabe

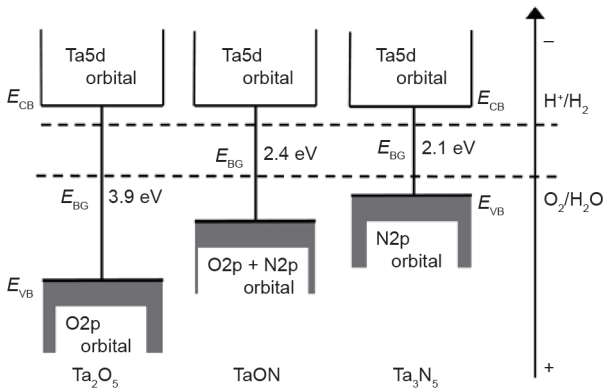

Fig. 3. Schematic band structures of Ta_2O_5, TaON, and Ta_3N_5 [54]. (Copyright 2003, American Chemical Society)

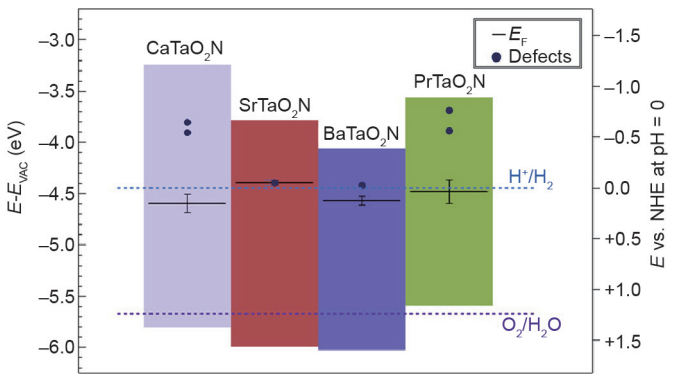

Fig. 4. Bandgap diagrams of tantalum-based oxynitride perovskite [55]. E_F: Femi lever; E_{VAC}: vacuum lever. (Copyright 2013, American Chemical Society)

[64] studied the effect of pressure on the final photocatalytic H_2 generation reaction of Ta_3N_5. It was demonstrated that Ta_3N_5 obtained under high-pressure ammonothermal treatment (> 50 MPa) showed improved photocatalytic H_2 evolution efficiency. The improved performance was attributed to the decrease of surface defects, which reduced surface recombination and improved the transfer of electrons to the surface active sites (platinum (Pt) co-catalyst or surface H^+). A higher density of defects was expected to cause stronger absorption at a wavelength longer than the absorption edge of the semiconductors [46,66–68]. Ta_3N_5 treated with an ammonia pressure of 50 MPa showed the lowest absorption intensity and the highest photocatalytic activity (Fig. 6) [64]. Thus, high-pressure ammonothermal treatment should be an effective way to suppress surface defects and enhance the photocatalytic activity of tantalum (oxy)nitride-based photocatalysts.

In addition to pressure, flux-assisted nitridation was adopted to synthesize the Ta_3N_5 photocatalysts with high crystallinity. Takata et al. [69] conducted a systematic study of flux-assisted nitridation for Ta_3N_5 preparation. Zinc (Zn), NaCl, and Na_2CO_3 were used as flux during the nitridation of Ta_2O_5 or $TaCl_5$ into Ta_3N_5. It was found that the introduction of NaCl and Na_2CO_3 as flux during the nitridation process led to the formation of morphologically defined particles. When $TaCl_5$ was nitrided along with NaCl, well-crystallized Ta_3N_5 nanoparticles were obtained (Fig. 7) [69]. In addition, the particle size could be controlled by varying the temperature. It was explained that nitridation and dissolution might happen simultaneously during flux-assisted nitridation, which would more effectively promote the diffusion of atoms in the materials. This result demonstrates that the morphology, dispersity, crystallinity, and surface states of tantalum (oxy)nitride can be controlled by varying the nitridation conditions, including temperature, ammonia pressure, precursor, and flux.

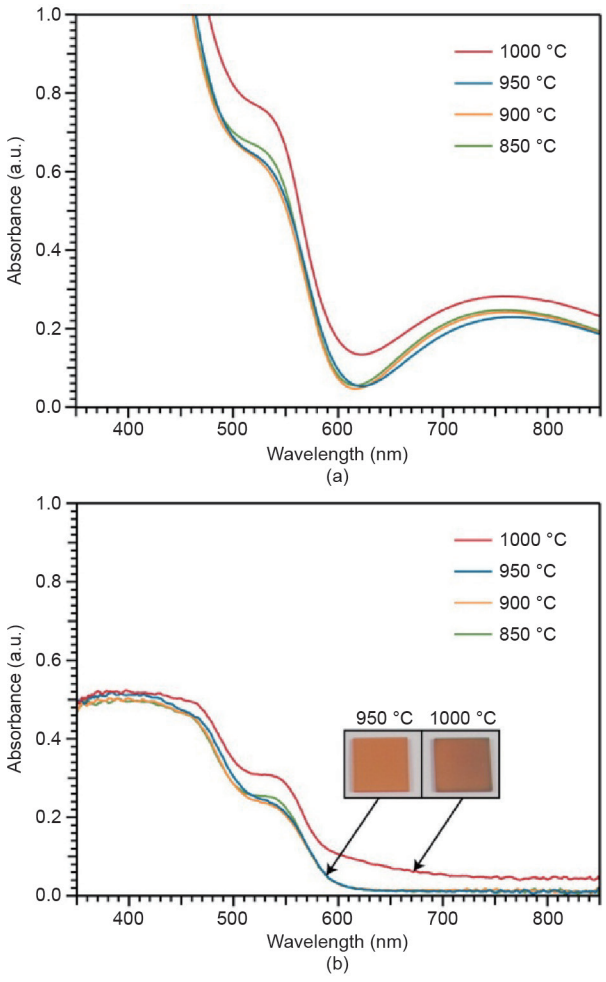

Fig. 5. UV-Vis light absorption spectra of Ta_3N_5 prepared at 850 °C, 900 °C, 950 °C, and 1000 °C in NH_3 gas collected in different mode: (a) transmission mode and (b) integrating sphere. Pictures inset in (b) show the gray tint in the sample treated at 950 °C and 1000 °C [62]. (Copyright 2014, American Chemical Society)

2.3. Strategies for improving water-splitting activity

The three main steps in photocatalytic water splitting, namely, light absorption, charge carrier migration, and surface redox reaction, have a synergistic effect on the activity of photocatalytic water splitting. Based on these three steps, many strategies including doping, morphological control, surface modification, co-catalyst design, and heterostructure design have been intensively explored in order to enhance the water-splitting activity of tantalum (oxy)nitride-based photocatalysts.

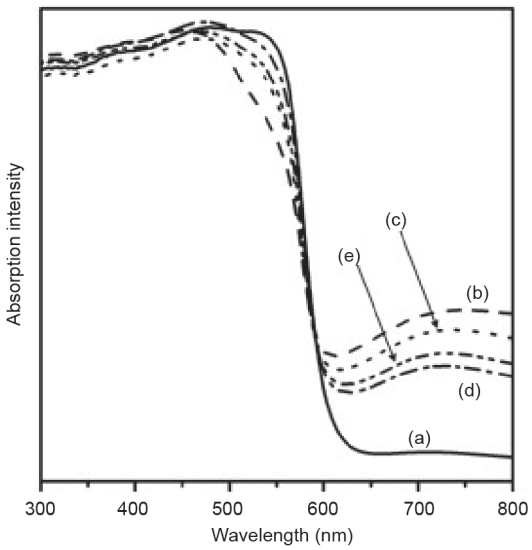

Fig. 6. UV-Vis light diffuse reflectance spectra of Ta_3N_5. (a) Pristine Ta_3N_5; (b–e) samples treated at 823 K for 5 h with (b) 10 MPa of N_2, (c) 10 MPa of NH_3, (d) 50 MPa of NH_3, and (e) 100 MPa of NH_3 [64]. (Copyright 2012, Elsevier)

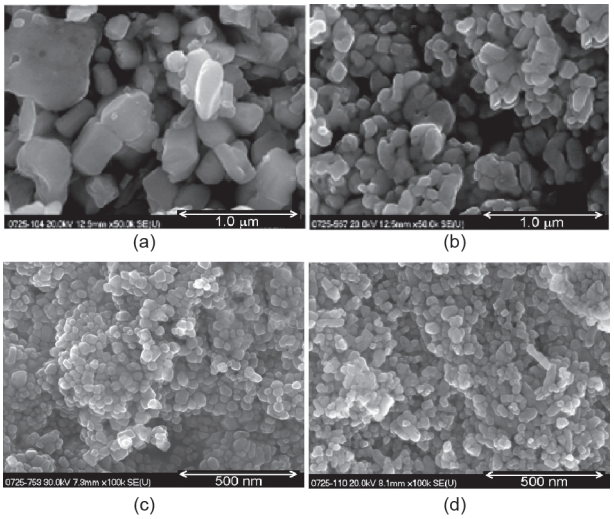

Fig. 7. Scanning electron microscope (SEM) images of Ta_3N_5 prepared by various flux-assisted nitridation methods. (a) Ta_2O_5-NaCl (850 °C for 10 h); (b) Ta_3N_5-NaCl (850 °C for 10 h); (c) $TaCl_5$-NaCl (800 °C for 10 h); (d) $TaCl_5$-Zn (800 °C for 10 h) [69]. (Copyright 2011, American Chemical Society)

2.3.1. Doping

Heteroatom doping is an important strategy to tune the basic properties of photocatalysts, such as bandgap structures, electronic conductivity, and surface structure. Doping is usually used to narrow the bandgap, increase the electronic conductivity, or make the surface active, thus promoting light harvesting, charge transfer reactions, and surface reactions. Through doping, the water-splitting performance of photocatalysts is significantly improved [70–75]. Foreign-ion-doped tantalum (oxy)nitride photoanodes or photocatalysts for O_2 evolution have been prepared and investigated intensively [76–80], but limited research attention has been paid to the H_2 evolution of doped tantalum (oxy)nitride-based photocatalysts. Seo et al. [81] systematically investigated magnesium (Mg)- and zirconium (Zr)-doped Ta_3N_5 photocatalysts for H_2 evolution. As shown in Fig. 8(a) [81], single substitution with Mg or Zr enhanced H_2 evolution by several times, while the activity of Ta_3N_5:Mg + Zr (doping concentration: 25 at%) for H_2 evolution was increased drastically, to approximately 15 times the performance of pure Ta_3N_5. According to the band structure investigation, the enhanced H_2 evolution activity was attributed to the negative shift of bandgap (Fig. 8(b)) [81]. The Mg + Zr co-doped Ta_3N_5 had a more negative CB and thus possessed a higher reduction potential, which favored water reduction.

When Mg ions were introduced into $LaTaON_2$, the resulting solid solution of $LaMg_xTa_{1-x}O_{1+3x}N_{2-3x}$ (x = 0–2/3) acted as a photocatalyst for water splitting at light absorptions up to 600 nm [21]. Further investigation revealed that the introduction of Mg ions enabled fine-tuning of the bandgap energy and positions, resulting from a co-substitution of Mg^{2+} for Ta^{5+} and O^{2-} for N^{3-}. As shown in Fig. 9(a) [82], the bandgap energy of $LaMg_xTa_{1-x}O_{1+3x}N_{2-3x}$ could easily be tuned by varying the Mg/(Mg + Ta) ratio. The absolute bandgap position of $LaMg_{0.33}Ta_{0.67}O_2N$ was revealed by combining photoelectron spectroscopy in air (PESA) with theoretical calculations. Both methods confirmed the negative shift of the CB and positive shift of the VB for $LaMg_{0.33}Ta_{0.67}O_2N$ compared with $LaTaON_2$ (Fig. 9(b)) [82]. An increased redox potential can enhance the water reduction and oxidation capability of photocatalysts, resulting in overall water splitting.

2.3.2. Morphological control

The morphology and particle size of the photocatalysts play important roles in charge separation and migration, as well as in surface reactions [12,83]. Smaller particle size means a shorter migration distance and a higher specific surface area. More photogenerated charge carriers can move to the surface and take part in the water redox reaction. Ta_3N_5 and TaON are typically obtained by the nitridation of Ta_2O_5 precursor. Various methods have been adopted to reduce the size of particles and control the morphology of the Ta_2O_5 precursor. However, phase transition occurs during high-temperature nitridation, which may cause the breakdown of nanostructures. Hisatomi et al. [84] solved this problem by coating the surface of the mesoporous Ta_2O_5 precursor with a silica layer before nitridation. The silica layer, which was obtained by chemical vapor deposition of tetramethyl orthosilicate, was used to support the mesoporous structure of Ta_2O_5 during high-temperature nitridation. As shown in Fig. 10(a) [84], ordered mesoporous Ta_3N_5 was obtained. The photocatalytic H_2 evolution efficiency was two times higher than that of conventional bulk Ta_3N_5, as a result of the thin-wall morphology. This ordered mesoporous structure had a wall thickness of 2 nm, a pore size of 4 nm, and a surface area as large

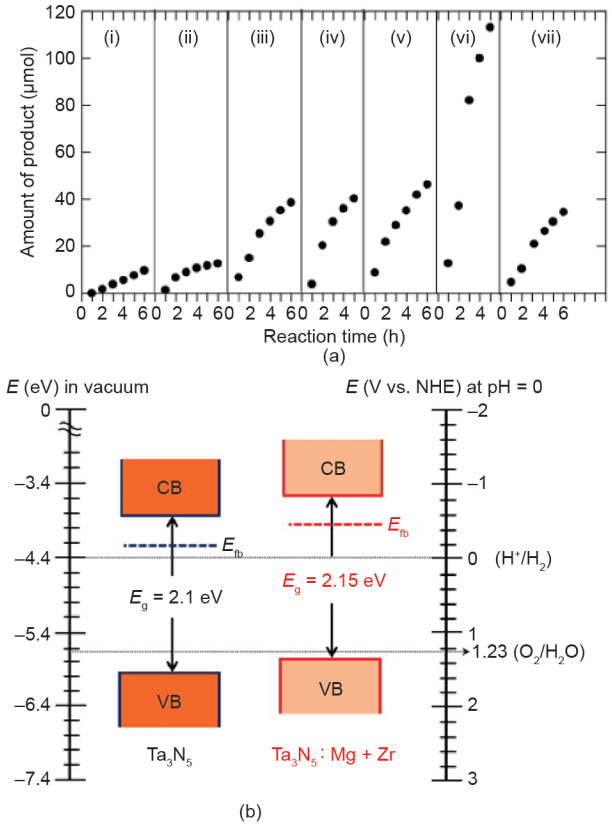

Fig. 8. (a) Time courses for photocatalytic H_2 production on Ta_3N_5 variants separately replaced with different amounts of Mg, Zr, or Mg + Zr: (i) undoped; (ii) 25 at% Mg; (iii) 40 at% Mg; (iv) 25 at% Zr; (v) 40 at% Zr; (vi) 25 at% Mg + Zr; (vii) 40 at% Mg + Zr. (b) Band structure diagram of Ta_3N_5 and Ta_3N_5:Mg + Zr [81]. E_{fb}: flat band energy. (Copyright 2015, American Chemical Society)

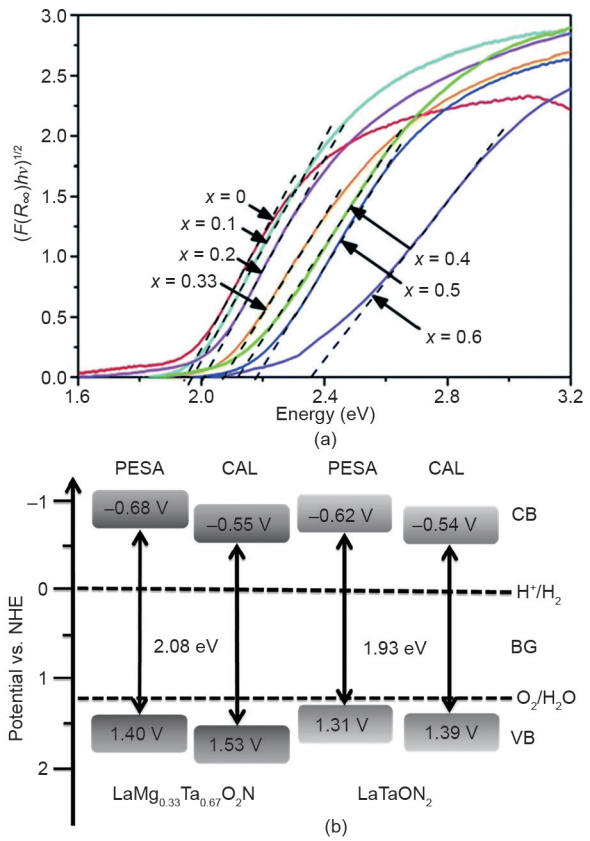

Fig. 9. (a) $(F(R_\infty)h\nu)^{1/2}$ versus the energy curve of $LaMg_xTa_{1-x}O_{1+3x}N_{2-3x}$ derived from UV-Vis light diffuse reflectance spectra. (b) Band levels of $LaMg_xTa_{1-x}O_{1+3x}N_{2-3x}$ (x = 0 and 0.33) obtained by PESA and theoretical calculations (CAL) [82]. (Copyright 2016, The Royal Society of Chemistry)

as 100 $m^2 \cdot g^{-1}$. Shorter charge migration distance and increased surface active sites contributed to the enhanced efficiency. The same group also reported a precursor route for preparing Ta_3N_5 nanoparticles (Fig. 10(b)) [85]. Ta_2O_5 nanoparticles, as a precursor for Ta_3N_5, were prepared using a precipitation method. With the particle size decreasing to 30–50 nm, the nanoparticulate Ta_3N_5 showed three times higher H_2 evolution activity than normal Ta_3N_5 (particle size 300–500 nm). The template-assisted method is another method of preparing nanostructured materials. The template not only acts as a model to control the morphology, but also acts as a support to prevent the Ta_2O_5 nanostructures from collapse during nitridation. By adopting mesoporous C_3N_4 as a template, Ta_3N_5 nanoparticles as small as 20 nm were obtained (Fig. 10(c)) [86]. Decreased particle size and increased surface area shortened the diffusion length of photo-excited electrons and holes, and further improved the charge carrier separation, making the resulting activity a magnitude higher than that of bulk Ta_3N_5. Similar to the silica nanosphere templates mentioned above, polystyrene (PS) spheres are also used as templates to synthesize microporous Ta_3N_5 (Fig. 10(d)) [87]. The PS sphere templates can easily be removed during calcination. The microporous structure and photonic behavior of the microporous Ta_3N_5 contributed to enhanced photon absorption and better performance [88,89].

In addition to nanoparticle and mesoporous structures, the construction of hierarchical nanostructures can effectively promote light harvesting and charge transfer. Hierarchical metastable γ-TaON structures have been reported as efficient H_2 evolution photocatalysts (Fig. 11) [90]. First, hierarchical Ta_2O_5 was prepared using an *in situ* self-assembly wet-chemical method. Next, a high-temperature nitridation process was used to transform Ta_2O_5 into TaON and Ta_3N_5. The hierarchical hollow structure of nano-needles that was assembled not only showed a large specific surface area but also led to multiple light reflections within the chamber. The obtained single-phase γ-TaON hierarchical structures exhibited a H_2 evolution rate of 381.6 $\mu mol \cdot h^{-1}$ and the apparent QE reached 9.5% (420 nm, ~47.5 times higher than that of traditional TaON). The converted Ta_3N_5 also showed improved photocatalytic H_2 evolution activity, reaching as high as 127.5 $\mu mol \cdot h^{-1}$ with an apparent QE of 3.1% (420 nm). The high efficiency is attributed to the synergistic effect of the hierarchical morphology and the crystal and electronic structures.

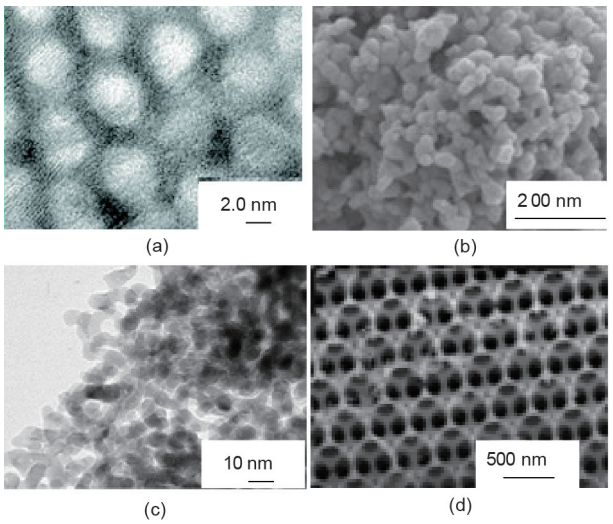

Fig. 10. (a) Transmission electron microscope (TEM) image of mesoporous Ta_3N_5 [84] (Copyright 2010, American Chemical Society); (b) SEM image of Ta_3N_5 nanoparticles prepared using the reverse homogeneous precipitation (RHP) method [85] (Copyright 2009, Elsevier); (c) TEM image of Ta_3N_5 particles prepared by adopting mesoporous C_3N_4 as the template [86] (Copyright 2010, The Royal Society of Chemistry); (d) SEM image of macroporous Ta_3N_5 [87] (Copyright 2012, Wiley-VCH).

On the other hand, use of a nanostructured Ta_2O_5 precursor can decrease the nitridation temperature and duration, which contributes to the maintenance of the nanostructure and decreases the amount of the Ta reduced species on the surface. Ordered porous Ta_2O_5 nanostructures were obtained from an ordered porous C_3N_4 template, which was prepared by using close-stacked silica nanospheres as templates [91]. It is important to note that this ordered porous structured Ta_2O_5 lowered the nitridation temperature, which resulted in a reduced extent of defect sites. Thus, the enhanced photocatalytic activity of the Ta_3N_5 photocatalyst obtained by this method was attributed to decreased defect sites, increased surface area, and efficient light harvesting. Similarly, the use of amorphous and shape-controlled Ta_2O_5 can decrease the nitridation time of Ta_3N_5, leading to fewer surface defects. Amorphous Ta_2O_5 nanoplates and octahedra were synthesized via aerosol-assisted molten salt syntheses (AMSS). The obtained porous Ta_3N_5 nanoplates and octahedra showed enhanced photocatalytic H_2 evolution rate, which could be attributed to suppression of the reduced Ta^{5+} surface states and increased surface area (Fig. 12) [92].

2.3.3. Surface modification

Nanostructures can decrease the distance migrated by the charge carrier and reduce body recombination. However, surface defects normally play the role of recombination centers for photo-excited charge carriers. Therefore, surface charge recombination is one of the major hazards for the photocatalytic performance of tantalum (oxy)nitride-based photocatalysts. However, reducing surface defects has been a challenge for tantalum (oxy)nitride-based photocatalysts [12]. ZrO_2 was reported to be an effective surface-passivated

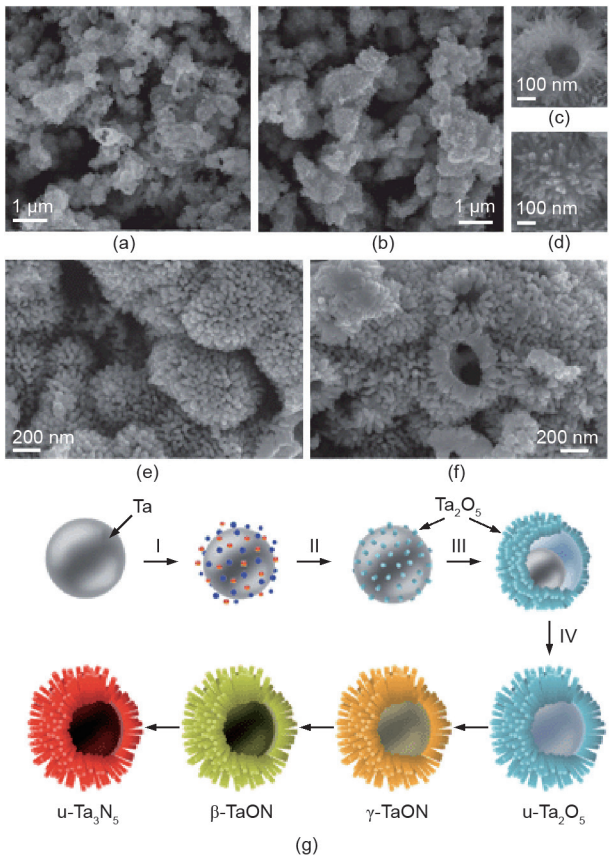

Fig. 11. SEM images of: (a–d) u-Ta_2O_5, (e) γ/β-TaON(u), and (f) u-Ta_3N_5. (g) Scheme of the formation of hollow urchin-like u-Ta_2O_5 hierarchical nanostructures and the subsequent thermal nitridation, successively forming γ-TaON, β-TaON, and u-Ta_3N_5 [90]. (Copyright 2013, The Royal Society of Chemistry)

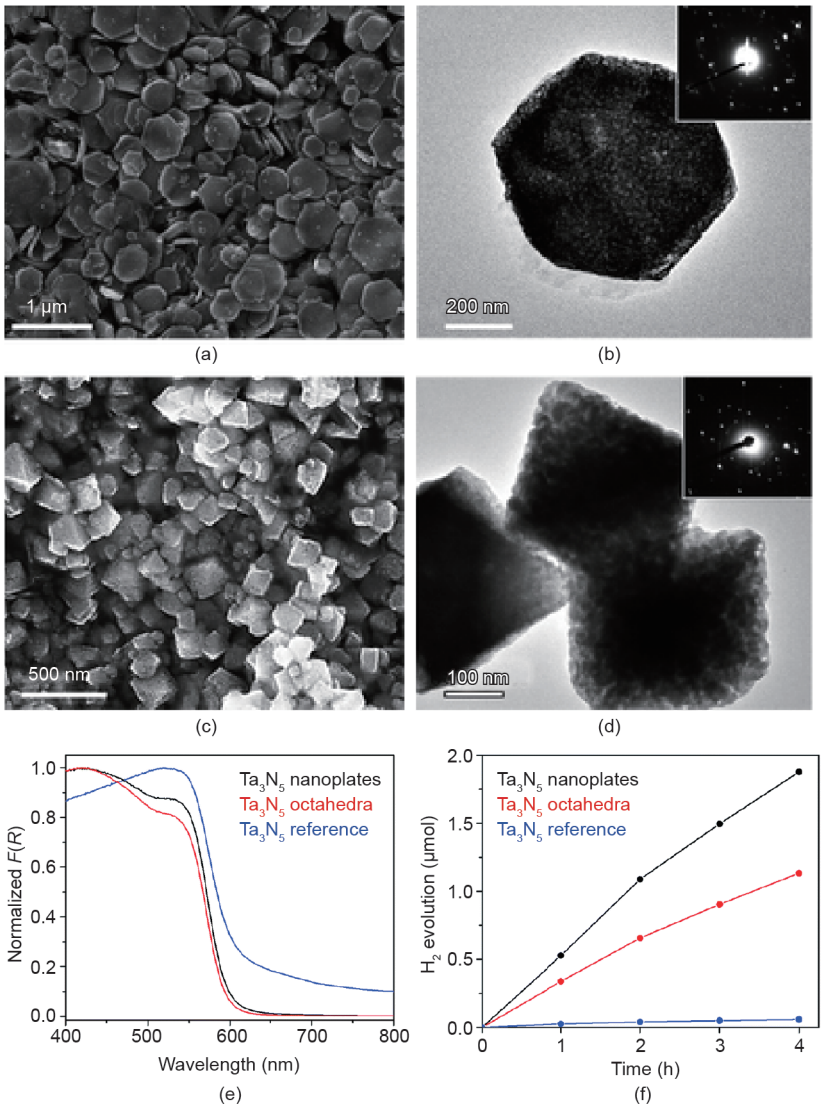

Fig. 12. (a, c) SEM and (b, d) TEM images (top right insets: electron diffraction) of (a, b) Ta_3N_5 nanoplates and (c, d) Ta_3N_5 octahedra. (e) Diffuse reflectance spectra and (f) time-dependent H_2 evolution reaction of different Ta_3N_5 samples [92]. (Copyright 2016, The Royal Society of Chemistry)

layer for TaON and Ta_3N_5 [93–96]. It was found that a solid solution formed between ZrO_2 and tantalum (oxy)nitride during the nitridation process. The solid solution on the surface could suppress the formation of reduced Ta species. Due to the decrease in reduced Ta species, ZrO_2-modified TaON and Ta_3N_5 photocatalysts showed an enhanced photocatalytic H_2 evolution rate. Another report about $BaTaO_2N$ may further elucidate the positive effect of surface modification [50]. Through the modification of a $BaTaO_x$ precursor with a Ba-Zr oxide species, a $BaZrO_3$-$BaTaO_2N$ solid solution formed after nitridation and showed six- to nine-fold enhancement of H_2 evolution without a sacrificial agent. This improved performance resulted from the enlarged bandgap and reduced defect density compared with bare $BaTaO_2N$, which led to an enhanced driving force for the water redox reaction and reduced charge recombination [85].

Self-oxidation and the reverse reaction are the main problems that impede the water-splitting activity of tantalum (oxy)nitride-based photocatalysts. A perovskite-type $CaTaO_2N$ photocatalyst was recently produced via appropriate surface modification, and was reported to exhibit overall photocatalytic water splitting (Fig. 13) [51]. $CaTaO_2N$ has a narrow bandgap and enough bandgap potential for water-splitting reactions (Fig. 13(a)) [51]. However, surface self-oxidation and the release of N_2 make this photocatalyst unstable. The surface of the $CaTaO_2N$ was modified with a thin layer of titanium oxyhydroxide through photodepostion, which effectively suppressed the surface self-oxidation and the reverse reaction. After loading the co-catalysts for the redox reactions, the modified $CaTaO_2N$ achieved stable overall water splitting (Fig. 13(b)) [51].

Depositing co-catalysts on the surface of photocatalysts is a general strategy to improve the water-splitting performance. However, surface states often result in the formation of an interface barrier between the co-catalyst and the photocatalyst, which is unfavorable for interfacial charge transfer. Chen et al. [97] reported that introducing a magnesia nanolayer between Pt nanoparticles and Ta_3N_5 could enhance the photocatalytic H_2 evolution efficiency significantly. The Pt/MgO-Ta_3N_5 photocatalysts reached 22.4 μmol·h^{-1} for H_2 evolution, which is about 17 times higher than the activity of the unmodified sample. It was found that the Pt nanoparticles deposited on MgO-Ta_3N_5 had a relatively small particle size and uniform dispersion, which resulted in more active sites and a faster surface reaction (Fig. 14(a, b)) [97]. This finding was attributed to the passivation of surface defects by MgO and the improvement of surface charge transfer from Ta_3N_5 to Pt. The same group further modified the

surface of Ta_3N_5 with barium (Ba) to promote the photocatalytic H_2 evolution rate, as shown in Fig. 14(c) [98]. It was found that $BaTaO_2N$ formed on the surface of Ta_3N_5 after modification with Ba. $BaTaO_2N$ not only passivated the surface defects but also formed a heterojunction with Ta_3N_5 (Fig. 14(d)) [98]. The improved photocatalytic H_2 evolution rate should be attributed to the synergetic effect of increased charge separation and decreased surface recombination.

2.3.4. Co-catalysts and heterostructures

Separating the photo-generated electrons and holes in different regions or sites to react with water by loading co-catalysts is an efficient way to increase photocatalytic efficiency [20,99–105]. Co-catalysts, which extract charge carriers from photocatalysts, show high catalytic activity for the water redox reaction. Faster extraction of charge carriers not only reduces bulk recombination but also suppresses the self-oxidation resulting from hole accumulation in the bulk, thereby improving the stability of tantalum (oxy)nitride-based photocatalysts. For example, Ta_3N_5 hollow spheres decorated with spatially separated co-catalysts were prepared with the assistance of silica spheres, and showed improved stability and enhanced H_2 evolution activity (Fig. 15) [40]. Pt nanoparticles were placed on the inner Ta_3N_5 shell surface as electron collectors, and IrO_2 or CoO_x nanoparticles were loaded on the outer shell surfaces as hole collectors (Fig. 15(a)) [40]. This hollow structure with separated co-catalysts has two advantages: ① It has an increased surface area and more active sites than bulk Ta_3N_5; and ② separated co-catalysts promote the migration and separation of photo-excited electrons and holes toward the inner and outer surfaces, respectively, thus suppressing recombination and reverse reactions. This system showed significant enhancement for photocatalytic water reduction (Fig. 15(d)) [40]. Moreover, no N_2 gas was detected during the H_2 evolution process, indicating improved stability.

As mentioned in Section 2.3.3, surface modification with ZrO_2 can suppress reduced Ta defects and enhance the water reduction performance of TaON. Therefore, ZrO_2/TaON was furthered modified with appropriate nanoparticulate co-catalysts for H_2 and O_2 evolutions, resulting in redox reagent-free overall water splitting (Fig. 16) [18]. As shown in Fig. 16(a) [18], the overall water-splitting reaction is affected by the synergistic combination of RuO_x, Cr_2O_3, and IrO_2. RuO_x loaded on a ZrO_2/TaON composite promoted both water reduction and oxidation activity [106]. Due to H_2-O_2 recombination to form H_2O and to the photoreduction of O_2 on the surface of RuO_x, a Cr_2O_3 shell that was permeable for protons and hydrogen, but not oxygen, was loaded onto the surface of RuO_x to prohibit the reverse reactions and make the overall water splitting achievable [107–110]. The function of IrO_2 is to improve the stability of the photocatalyst. The authors attributed the improved stability to the promotion of water oxidation by IrO_2, which is known to be the most effective catalyst for O_2 evolution [111–113]. Thus, the overall water-splitting reaction on the composite photocatalyst $IrO_2/Cr_2O_3/RuO_x/ZrO_2$/TaON can provide some useful insight into the reasonable design of a functional co-catalysts/photocatalyst system.

Combining different materials to form heterostructured photocatalysts is another effective strategy to improve water-splitting performance, due to the improvement of photon absorption and charge separation [5,11]. Numerous composite photocatalysts, including Cu_2O/TiO_2, TiO_2/CdS, and CdS/WO_3, were combined and showed remarkably improved photocatalytic performance

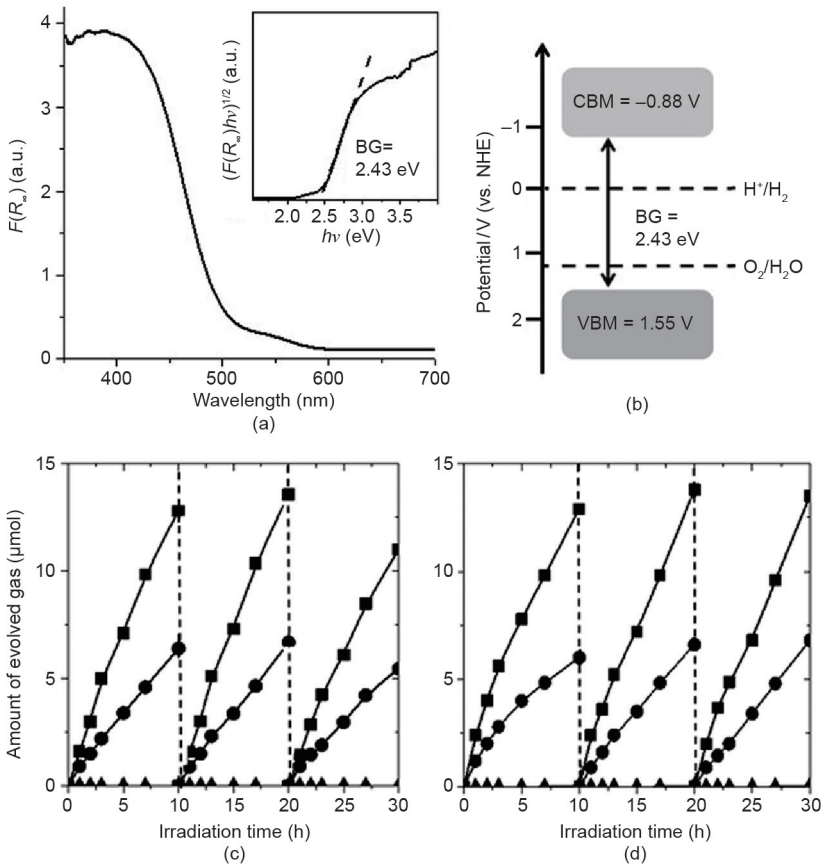

Fig. 13. (a) UV-Vis diffuse reflectance spectra (inset: Tauc plot) and (b) band position of $CaTaO_2N$ as determined by calculation. Time courses of gas evolution during water splitting on titanium-oxyhydroxide-deposited $RhCrO_y/CaTaO_2N$ under (c) UV + Visible light ($\lambda \geq 300$ nm) and (d) visible light ($\lambda \geq 420$ nm) [51]. (Copyright 2015, The Royal Society of Chemistry)

compared with single-component photocatalysts [114–117]. Increasing efforts have been made to construct tantalum (oxy)nitride-based heterostructured photocatalysts. Liu et al. [118] reported a nano Au/Ta_3N_5 composite as a photocatalyst for H_2 generation under visible-light irradiation. The nano Au/Ta_3N_5 composite was prepared through nitridation of Au/Ta_2O_5, which was synthesized via a simple Pechini-type sol-gel process. Gold (Au) nanoparticles with a diameter of 15–20 nm were embedded in the Ta_2O_5 host (Fig. 17(a,b)) [119]. The prepared nano Au/Ta_3N_5 heterostructures showed remarkably improved H_2 evolution performance under visible-light irradiation compared with pure Ta_3N_5 nanoparticles. The authors attributed the enhanced H_2 evolution activity to the synergetic effect of a near-field electromagnetic effect induced by the surface plasmon resonance of Au nanoparticles (Fig. 17(c)) and charge transfer in the Au/Ta_3N_5 composite. Fig. 17(d) [119] shows the time course of H_2 evolution for the Au/Ta_3N_5 composite photocatalysts. A certain amount of Au nanoparticles can enhance the photocatalytic H_2 evolution performance, whereas excessive Au nanoparticles may act as recombination centers and impede the photocatalytic H_2 evolution activity [119].

Heterojunctions formed between two photocatalysts with suitable bandgaps and matched band positions have been demonstrated to be effective for improving photocatalytic performance [120]. Adhikari et al. [121] reported the composites of Ta_3N_5 or TaON with Bi_2O_3 to have enhanced visible-light-driven H_2 evolution activity. They ascribed the increased visible-light activity for Ta_3N_5 or TaON to the trapping of holes by Bi_2O_3. Under visible-light irradiation, both Ta_3N_5 and Bi_2O_3 were excited to generate electrons and holes. The electrons from Ta_3N_5 or TaON took part in the H_2 evolution activity and holes were recombined with the electrons from Bi_2O_3, similar to the Z-scheme mechanism shown in Fig. 18 [121]. In other words, the enhanced H_2 evolution activity of Bi_2O_3/Ta_3N_5 or Bi_2O_3/TaON composites could be attributed to improved charge separation [121].

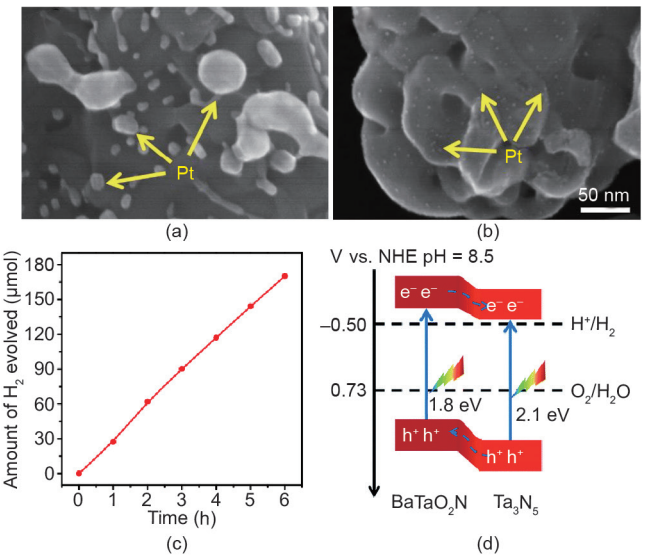

Fig. 14. Field emission scanning electron microscope (FESEM) images of (a) Pt/Ta_3N_5 and (b) Pt/MgO(in)-Ta_3N_5 [97] (Copyright 2016, Elsevier); (c) Time course of visible-light H_2 evolution with 0.5 wt% Pt/Ba(0.3)-Ta_3N_5; (d) relative band positions of the $Ta_3N_5/BaTaO_2N$ heterostructure [98] (Copyright 2017, The Royal Society of Chemistry).

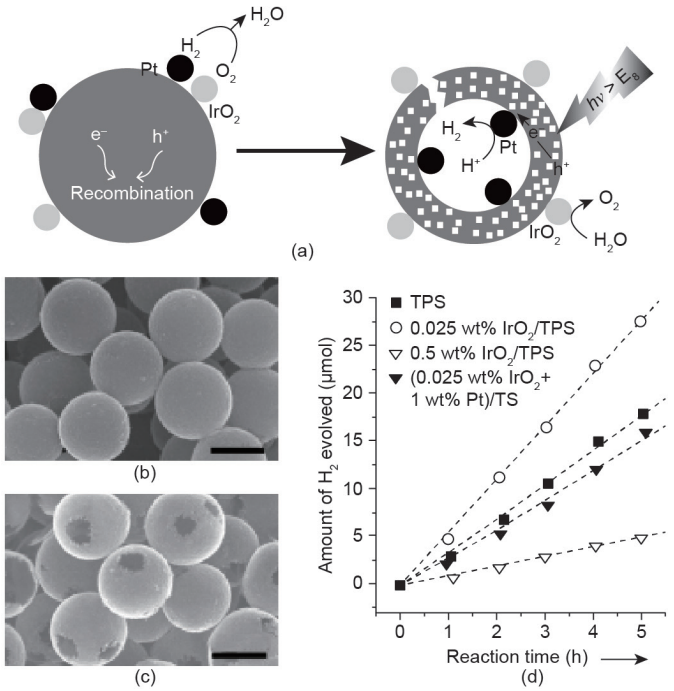

Fig. 15. (a) Scheme illustration of two separated co-catalysts used to decorate Ta_3N_5 hollow spheres to create an effective photocatalyst for water splitting. (b,c) SEM images of (b) $Ta_3N_5/Pt/SiO_2$ spheres and (c) Ta_3N_5/Pt hollow spheres. The scale bar is 500 nm. (d) Time course of H_2 evolution on Ta_3N_5 photocatalysts with and without spatially separated co-catalysts [40]. TPS: $Ta_3N_5/Pt/SiO_2$; TS: Ta_3N_5/SiO_2. (Copyright 2013, Wiley-VCH)

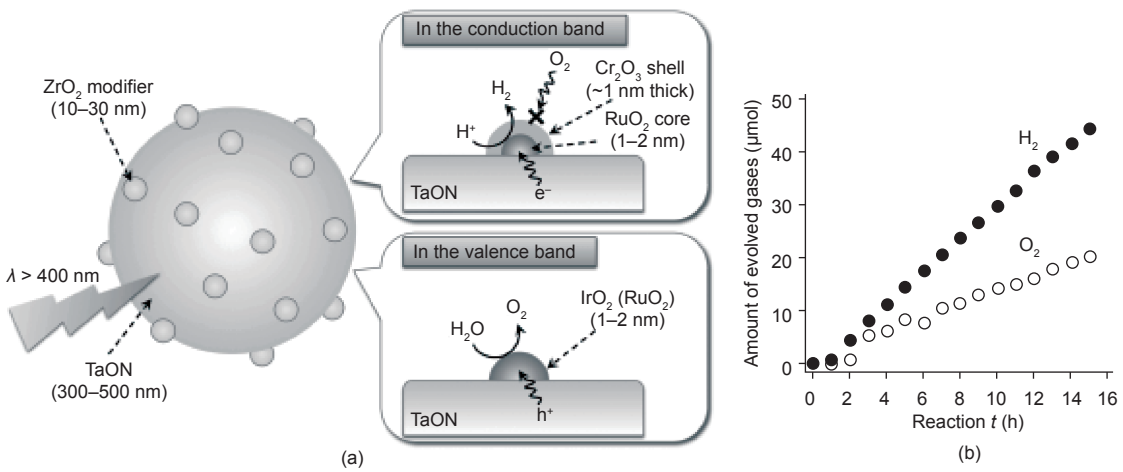

Fig. 16. (a) Scheme of the mechanism of overall water splitting on an $IrO_2/Cr_2O_3/RuO_x/ZrO_2$/TaON photocatalyst. (b) Time course of gas evolution using $IrO_2/Cr_2O_3/RuO_x$/TaON under visible light (λ > 400 nm) [18]. (Copyright 2013, Wiley-VCH)

As the bandgaps of most tantalum (oxy)nitride-based photocatalysts straddle water redox potentials, tantalum (oxy)nitride-based photocatalysts can act as both H_2 evolution photocatalysts (HEPs) and as O_2 evolution photocatalysts (OEPs) in a Z-scheme system. For example, Higashi et al. [122] designed a Z-scheme system with TaON photocatalysts to achieve visible-light overall water splitting. As shown in Fig. 19(a) [122], the TaON acted as both HEP and OEP after the loading of appropriate co-catalysts. With the assistance of an IO_3^-/I^- redox mediator, the Pt/TaON (HEP) and RuO_2/TaON (OEP) mixtures reacted with water to produce H_2 and O_2 under visible-light irradiation. Later, Tabata et al. [123] further decorated the surface of Ta_3N_5 with rutile titania (R-TiO_2), which acted as an OEP in a two-step water-splitting system (Fig. 19(b)). After the loading of iridium (Ir) nanoparticles, Ir/R-TiO_2/Ta_3N_5 achieved visible-light overall water splitting along with Pt/ZrO_2/TaON as a HEP, assisted by an IO_3^-/I^- redox mediator. It was believed that the decorated R-TiO_2 hindered the adsorption of I^- on Ta_3N_5, while the Ir nanoparticles played the role of active sites to reduce IO_3^- to I^-, thereby allowing Ta_3N_5 to evolve O_2 in the two-step water-splitting system.

2.4. Performance of tantalum (oxy)nitride-based photocatalysts

To improve the water-splitting efficiency, great effort has been focused on each step of the photocatalytic process, including photon absorption, charge separation and migration, and surface reaction. The main strategies—doping, morphological control, surface modification, co-catalysts, and heterostructures—are discussed above. High activity and stability for photocatalysts are based on the synergistic

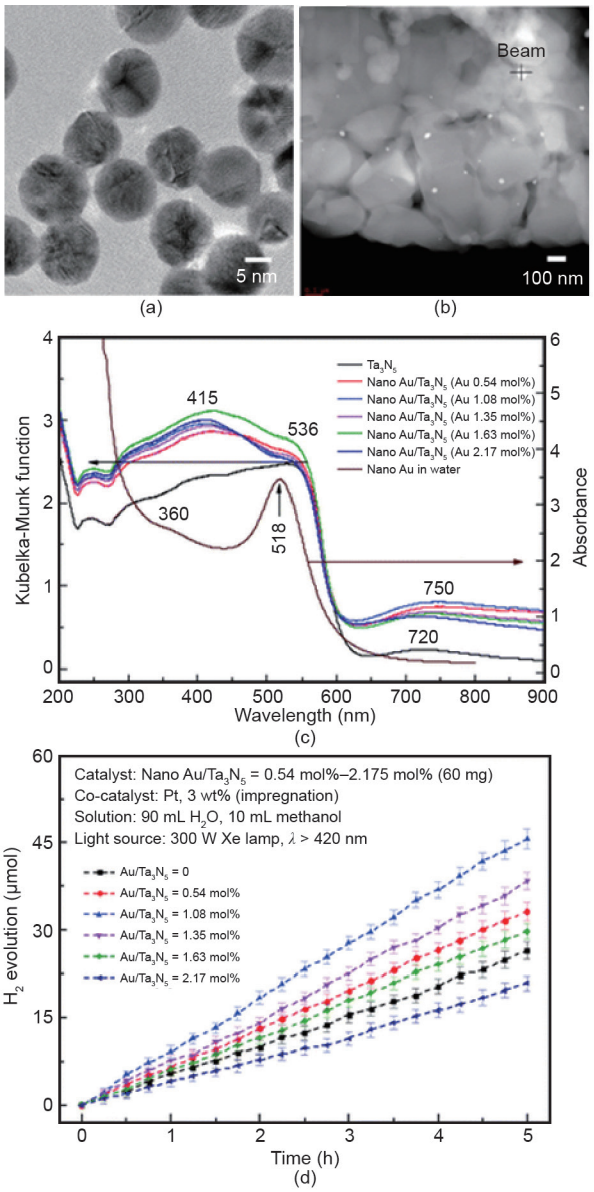

Fig. 17. (a) A TEM image of Au nanoparticles; (b) high-angle annular dark-field scanning transmission electron microscope (STEM) image of nano Au/Ta_3N_5; (c) the UV-Vis diffuse reflectance spectra of nano Au/Ta_3N_5; (d) the time course of H_2 evolution for the nano Au/Ta_3N_5 composites [119]. (Copyright 2014, The Royal Society of Chemistry)

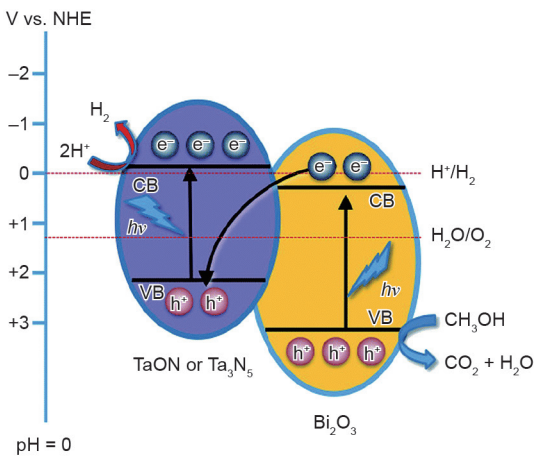

Fig. 18. Relative bandgap positions and charge transfer mechanism (Z-scheme) in Bi_2O_3 and Ta_3N_5 under visible-light irradiation [121]. (Copyright 2015, The Royal Society of Chemistry)

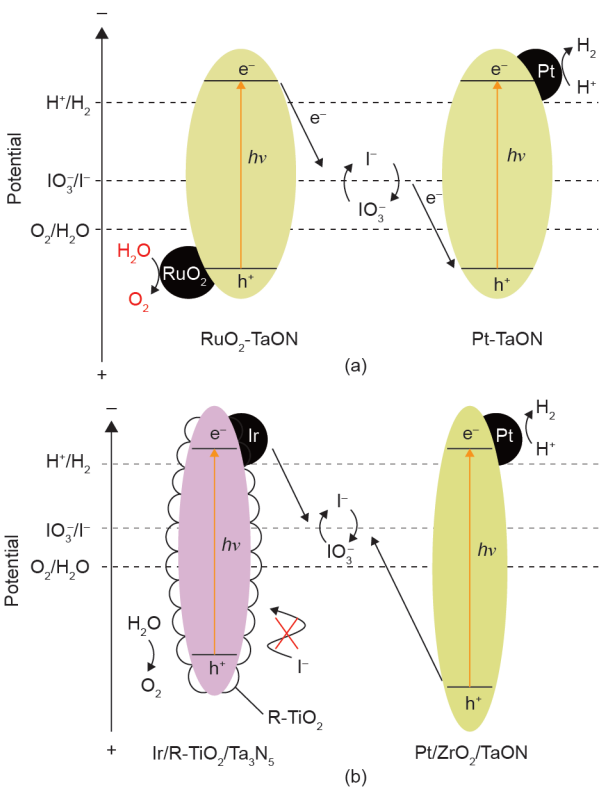

Fig. 19. (a) Scheme of the Z-scheme overall water splitting on a RuO_2/TaON and Pt/TaON mixture with an IO_3^-/I^- redox mediator [122] (Copyright 2008, The CSJ Journals); (b) Scheme of two-step water splitting on a Pt/ZrO_2/TaON and Ir/R-TiO_2/Ta_3N_5 mixture with an IO_3^-/I^- redox mediator [123] (Copyright 2010, American Chemical Society).

effect of these steps. Photocatalytic overall water splitting has been achieved on modified TaON, $CaTaO_2N$, and $LaMg_xTa_{1-x}O_{1+3x}N_{2-3x}$. Table 2 [18,21,40,43,51,63,65,81,84,87,90,92,96–99,118,119] summarizes and compares relevant studies on this topic. It is clear that nanostructures show relatively higher H_2 evolution performance due to the increased number of active sites and the short charge transfer distance. In addition, heteroatoms-doping that is based on bandgap engineering is an effective strategy to enhance the H_2 evolution performance of tantalum (oxy)nitride-based photocatalysts. However, a greater surface area means more surface defects, which not only act as recombination centers but also impede the photo-excited charge transfer between the photocatalyst and the co-catalyst. Also, the heteroatom dopant may act as a recombination center. Thus, surface modification seems to be a more powerful strategy for the improvement of the H_2 evolution performance of tantalum (oxy) nitride photocatalysts.

3. Conclusions and outlook

Tantalum (oxy)nitride-based photocatalysts, which have a narrow bandgap for visible-light absorption and suitable bandgap edges for the water redox reaction, are regarded as a class of promising candidates for water splitting. Because they have much lower water reduction capability than water oxidation capability, considerable attention has been devoted to the improvement of the photocatalytic H_2-generation efficiency of tantalum (oxy)nitride-based photocatalysts. Surface states are considered to be a major factor influencing photocatalytic water-splitting activity. Surface defects caused by nitrogen vacancies and Ta reduced species act as recombination centers and impede the surface charge transfer and reaction. In addition, self-oxidation and the reverse reaction during a photocatalytic reaction make these photocatalysts unstable. In order to improve the water-splitting performance of tantalum (oxy)nitride-based photocatalysts, many strategies have been adopted, including doping, morphology control, surface modification, co-catalysts, and heterostructures design. These strategies work by improving charge separation, charge migration, and surface reactions. Photocatalytic overall water splitting has been achieved on some tantalum (oxy)nitride-based photocatalysts. In addition, the stability of tantalum (oxy)nitride-based photocatalysts has been significantly improved with appropriate co-catalyst design and surface modification.

To further improve the photocatalytic overall water-splitting efficiency of tantalum (oxy)nitride-based photocatalysts, increased attention should be paid to better designing and utilizing the synergistic effect of various strategies. The following key points should be considered in future research.

(1) Defects control. It is believed that most defects on the surface or in the bulk will act as recombination centers for photo-excited electrons and holes. Moreover, surface defects may generate interfacial barriers between the photocatalysts and the co-catalysts, and impede charge transfer. It is very important but quite challenging to reduce the defects because of the harsh nitridation conditions. It is easy to introduce nitrogen vacancies and Ta reduced species during the high-temperature nitridation process in a NH_3 atmosphere. The exploration of new precursors and synthesis methods under mild conditions is necessary in order to reduce the defects of tantalum (oxy)nitride-based photocatalysts.

(2) Morphology control. The morphology of photocatalysts is a key factor that influences light absorption, charge migration, and surface reaction. Nanotechnology has been intensively used to design various photocatalysts, and for the most important aspect of morphology control. Reducing the particle size to the nanoscale results in a shorter migration distance that makes more charge carriers move to the surface before recombination. Furthermore, nanostructures decrease the temperature and duration of nitridation, which reduces defects such as nitrogen vacancies and Ta reduced species. In addition, ordered porous nanostructures increase light absorption because of the photonic effect. An ordered hierarchical

Table 2
Tantalum (oxy)nitride-based photocatalysts for water splitting.

Photocatalysts	Morphology	Co-catalyst (Amount, wt%)	Light source	Reaction solution	Activity (μmol·(g·h)$^{-1}$)		Ref.
					H_2	O_2	
Ta_3N_5	Microparticles	Pt (3.0)	300 W Xe (λ > 420 nm)	Methanol	9.0	NA	[43]
Ta_3N_5	Nanoparticles	Pt (0.5)	300 W Xe (λ > 420 nm)	Methanol	10.5	NA	[85]
Ta_3N_5	Mesoporous	Pt (3.0)	300 W Xe (λ > 420 nm)	Methanol	17.0	NA	[84]
Ta_3N_5	Microparticles	Pt (0.5)	300 W Xe (λ > 420 nm)	Methanol	110.0	NA	[65]
Ta_3N_5	Nanoparticles	Pt (0.5)	450 W Hg (λ > 400 nm)	Methanol	136.0	NA	[86]
Ta_3N_5	Ordered porous	Pt (3.0)	300 W Xe (λ > 420 nm)	Methanol	18.0	NA	[91]
Ta_3N_5	Microparticles	Pt (0.5)	70 W halide (λ > 380 nm)	Methanol	72.0	NA	[64]
Ta_3N_5	Hollow structure	Pt (0.1)	300 W Xe (λ > 420 nm)	Methanol	425.0	NA	[90]
Ta_3N_5	Hollow spheres	Pt (1) IrO_2 (0.025)	300 W Xe (λ > 420 nm)	Methanol	206.3	NA	[40]
Ta_3N_5	Nanoplates	Pt (3.0)	300 W Xe (λ > 400 nm)	Methanol	26.5	NA	[92]
Ta_3N_5	Macroporous	NA	300 W Xe	Methanol	82.5	NA	[87]
Mg-Ta_3N_5	Microparticles	Pt (0.3)	300 W Xe (λ > 420 nm)	Methanol	70.4	NA	[81]
Zr-Ta_3N_5	Microparticles	Pt (0.3)	300 W Xe (λ > 420 nm)	Methanol	80.6	NA	[81]
(Mg + Zr)-Ta_3N_5	Microparticles	Pt (0.3)	300 W Xe (λ > 420 nm)	Methanol	60.8	NA	[81]
SiO_2/Ta_3N_5	Core/shell	Pt (3.0)	300 W Xe (λ > 420 nm)	Methanol	83.3	NA	[118]
ZrO_2/Ta_3N_5	Microparticles	Pt (0.5)	300 W Xe (λ > 420 nm)	Methanol	27.4	NA	[96]
MgO/Ta_3N_5	Microparticles	Pt (2.0)	300 W Xe (λ > 420 nm)	Methanol	149.3	NA	[97]
$BaTaO_2N/Ta_3N_5$	Microparticles	Pt (0.5)	300 W Xe (λ > 420 nm)	Methanol	201.3	NA	[98]
Au/Ta_3N_5	Nanoparticles	Pt (1.0)	300 W Xe (λ > 420 nm)	Methanol	150.0	NA	[119]
ZrO_2/TaON	Nanoparticles	$IrO_2/Cr_2O_3/RuO_x$ (3.0)	450 W Hg (λ > 400 nm)	Water	15.0	6.70	[18]
$LaMg_{1/3}Ta_{2/3}ON$	Nanoparticles	$RhCrO_y$ (0.5)	300 W Xe (λ > 420 nm)	Water	5.0	2.50	[21]
$CaTaO_2N$	Nanoparticles	$RhCrO_y$	300 W Xe (λ > 420 nm)	Water	0.7	0.35	[51]

structure will provide room for improving the water-splitting activity of tantalum (oxy)nitride-based photocatalysts.

(3) Co-catalyst design. Loading co-catalysts is an effective approach to improve photocatalytic performance. Tantalum (oxy)nitride-based photocatalysts suffer from self-oxidation during the photocatalytic process, as a result of the poor extraction of photo-generated holes. The loading of a co-catalyst for water oxidation can promote the extraction of holes and improve the stability of photocatalysts. Precise control of the particle size and dispersion of co-catalysts should show a positive effect on the stability and performance of the photocatalyst. Thus far, Pt is the most-used H_2 evolution co-catalyst for Ta_3N_5 based photocatalysts. However, due to its rarity and high cost, Pt is not favorable for scale-up applications. Therefore, the development of other earth-abundant co-catalysts for H_2 evolution is greatly welcome.

In conclusion, much effort has been made to improve the water-splitting efficiency of tantalum (oxy)nitride-based photocatalysts, and great progress has been achieved over the past years. Due to the synergetic effect of light harvesting, charge separation and migration, and surface reaction during the photocatalytic water-splitting process, more research attention should be paid to combining strategies into multi-strategies. Persistent efforts in this area are expected to realize highly efficient overall water splitting on these photocatalysts. Furthermore, the knowledge and understanding of mechanisms that have been acquired from studying these materials will shed light on the development of other new, efficient, and sustainable photocatalysts. For the future development of photocatalytic water splitting, unified evaluation standards and criteria for overall photocatalyst performance, including efficiency and stability, are urgently required to allow this research community to achieve its ambition of long-term sustainable solar fuel production.

Acknowledgements

The authors would like to acknowledge financial support from the Australian Research Council through its DP and FF programs. Mu Xiao acknowledges support from the Australian Government Research Training Program Scholarship. Financial support from the National Natural Science Foundation of China (513228201) is also highly appreciated.

Compliance with ethics guidelines

Mu Xiao, Songcan Wang, Supphasin Thaweesak, Bin Luo, and Lianzhou Wang declare that they have no conflict of interest or financial conflicts to disclose.

References

[1] Dunn S. Hydrogen futures: Toward a sustainable energy system. Int J Hydrogen Energy 2002;27(3):235–64.
[2] Graetz J. New approaches to hydrogen storage. Chem Soc Rev 2009;38(1):73–82.
[3] Holladay JD, Hu J, King DL, Wang Y. An overview of hydrogen production technologies. Catal Today 2009;139(4):244–60.
[4] Conte M, Prosini PP, Passerini S. Overview of energy/hydrogen storage: State-of-the-art of the technologies and prospects for nanomaterials. Mater Sci Eng B 2004;108(1–2):2–8.
[5] Moniz SJA, Shevlin SA, Martin DJ, Guo ZX, Tang J. Visible-light driven heterojunction photocatalysts for water splitting—A critical review. Energy Environ Sci 2015;8(3):731–59.
[6] Acar C, Dincer I, Naterer GF. Review of photocatalytic water-splitting methods for sustainable hydrogen production. Int J Energy Res 2016;40(11):1449–73.
[7] Jafari T, Moharreri E, Amin A, Miao R, Song W, Suib S. Photocatalytic water splitting—The untamed dream: A review of recent advances. Molecules 2016;21(7):900.
[8] Chen S, Thind SS, Chen A. Nanostructured materials for water splitting-state of the art and future needs: A mini-review. Electrochem Commun 2016;63:10–7.
[9] Chen J, Zhao D, Diao Z, Wang M, Shen S. Ferrites boosting photocatalytic hydrogen evolution over graphitic carbon nitride: A case study of (Co, Ni)Fe_2O_4 modification. Sci Bull 2016;61(4):292–301.
[10] Liu Y, Tian L, Tan X, Li X, Chen X. Synthesis, properties, and applications of black titanium dioxide nanomaterials. Sci Bull 2017;62(6):431–41.
[11] Kudo A, Miseki Y. Heterogeneous photocatalyst materials for water splitting. Chem Soc Rev 2009;38(1):253–78.
[12] Tong H, Ouyang S, Bi Y, Umezawa N, Oshikiri M, Ye J. Nano-photocatalytic materials: Possibilities and challenges. Adv Mater 2012;24(2):229–51.
[13] Hisatomi T, Kubota J, Domen K. Recent advances in semiconductors for photocatalytic and photoelectrochemical water splitting. Chem Soc Rev 2014;43(22):7520–35.
[14] Zhang P, Zhang J, Gong J. Tantalum-based semiconductors for solar water splitting. Chem Soc Rev 2014;43(13):4395–422.
[15] Zou Z, Ye J, Sayama K, Arakawa H. Direct splitting of water under visible light irradiation with an oxide semiconductor photocatalyst. Nature 2001;414(6864):625–7.
[16] Maeda K, Teramura K, Lu D, Takata T, Saito N, Inoue Y, et al. Photocatalyst releasing hydrogen from water. Nature 2006;440(7082):295.
[17] Lee Y, Terashima H, Shimodaira Y, Teramura K, Hara M, Kobayashi H, et al. Zinc germanium oxynitride as a photocatalyst for overall water splitting under visible light. J Phys Chem C 2007;111(2):1042–8.
[18] Maeda K, Lu D, Domen K. Direct water splitting into hydrogen and oxygen under visible light by using modified TaON photocatalysts with d^0 electronic configuration. Chemistry 2013;19(16):4986–91.
[19] Liu J, Liu Y, Liu N, Han Y, Zhang X, Huang H, et al. Metal-free efficient photocatalyst for stable visible water splitting via a two-electron pathway. Science 2015;347(6225):970–4.
[20] Meng A, Zhang J, Xu D, Cheng B, Yu J. Enhanced photocatalytic H_2-production activity of anatase TiO_2 nanosheet by selectively depositing dual-cocatalysts on (101) and (001) facets. Appl Catal B 2016;198:286–94.
[21] Pan C, Takata T, Nakabayashi M, Matsumoto T, Shibata N, Ikuhara Y, et al. A complex perovskite-type oxynitride: The first photocatalyst for water splitting operable at up to 600 nm. Angew Chem Int Ed 2015;54(10):2955–9.
[22] Li Q, Guo B, Yu J, Ran J, Zhang B, Yan H, et al. Highly efficient visible-light-driven photocatalytic hydrogen production of CdS-cluster-decorated graphene nanosheets. J Am Chem Soc 2011;133(28):10878–84.
[23] Frame FA, Osterloh FE. CdSe-MoS_2: A quantum size-confined photocatalyst for hydrogen evolution from water under visible light. J Phys Chem C 2010;114(23):10628–33.
[24] Tsuji I, Kato H, Kudo A. Visible-light-induced H_2 evolution from an aqueous solution containing sulfide and sulfite over a ZnS-$CuInS_2$-$AgInS_2$ solid-solution photocatalyst. Angew Chem Int Ed 2005;117(23):3631–4.
[25] Yoneyama H. Electrochemical aspects of light-induced heterogeneous reactions on semiconductors. Crit Rev Solid State Mater Sci 1993;18(1):69–111.
[26] Kazunari D, Kondo JN, Michikazu H, Tsuyoshi T. Photo- and mechano-catalytic overall water splitting reactions to form hydrogen and oxygen on heterogeneous catalysts. Bull Chem Soc Jpn 2000;73(6):1307–31.
[27] Kudo A. Development of photocatalyst materials for water splitting. Int J Hydrogen Energy 2006;31(2):197–202.
[28] Shangguan W. Hydrogen evolution from water splitting on nanocomposite photocatalysts. Sci Technol Adv Mater 2007;8(1–2):76–81.
[29] Kudo A. Recent progress in the development of visible light-driven powdered photocatalysts for water splitting. Int J Hydrogen Energy 2007;32(14):2673–8.
[30] Maeda K, Domen K. New non-oxide photocatalysts designed for overall water splitting under visible light. J Phys Chem C 2007;111(22):7851–61.
[31] Osterloh FE. Inorganic nanostructures for photoelectrochemical and photocatalytic water splitting. Chem Soc Rev 2013;42(6):2294–320.
[32] Cao S, Low J, Yu J, Jaroniec M. Polymeric photocatalysts based on graphitic carbon nitride. Adv Mater 2015;27(13):2150–76.
[33] Zhang G, Liu G, Wang L, Irvine JTS. Inorganic perovskite photocatalysts for solar energy utilization. Chem Soc Rev 2016;45(21):5951–84.
[34] Xu Y, Kraft M, Xu R. Metal-free carbonaceous electrocatalysts and photocatalysts for water splitting. Chem Soc Rev 2016;45(11):3039–52.
[35] Yuan L, Han C, Yang MQ, Xu YJ. Photocatalytic water splitting for solar hydrogen generation: Fundamentals and recent advancements. Int Rev Phys Chem 2016;35(1):1–36.
[36] Grätzel M. Photoelectrochemical cells. Nature 2001;414(6861):338–44.
[37] Walter MG, Warren EL, McKone JR, Boettcher SW, Mi Q, Santori EA, et al. Solar water splitting cells. Chem Rev 2010;110(11):6446–73.
[38] Li Z, Luo W, Zhang M, Feng J, Zou Z. Photoelectrochemical cells for solar hydrogen production: Current state of promising photoelectrodes, methods to improve their properties, and outlook. Energy Environ Sci 2013;6(2):347–70.
[39] Murphy AB, Barnes PRF, Randeniya LK, Plumb IC, Grey IE, Horne MD, et al. Efficiency of solar water splitting using semiconductor electrodes. Int J Hydrogen Energy 2006;31(14):1999–2017.
[40] Wang D, Hisatomi T, Takata T, Pan C, Katayama M, Kubota J, et al. Core/shell photocatalyst with spatially separated co-catalysts for efficient reduction and oxidation of water. Angew Chem Int Ed 2013;52(43):11252–6.
[41] Nurlaela E, Ziani A, Takanabe K. Tantalum nitride for photocatalytic water splitting: Concept and applications. Mater Renew Sust Energy 2016;5(4):18.
[42] Moriya Y, Takata T, Domen K. Recent progress in the development of (oxy) nitride photocatalysts for water splitting under visible-light irradiation. Coord Chem Rev 2013;257(13–14):1957–69.
[43] Go H, Akio I, Tsuyoshi T, Kondo JN, Michikazu H, Kazunari D. Ta_3N_5 as a novel visible light-driven photocatalyst (λ < 600 nm). Chem Lett 2002;31(7):736–7.
[44] Nurlaela E, Ould-Chikh S, Llorens I, Hazemann JL, Takanabe K. Establishing

efficient cobalt-based catalytic sites for oxygen evolution on a Ta_3N_5 photocatalyst. Chem Mater 2015;27(16):5685–94.
[45] Chen S, Shen S, Liu G, Qi Y, Zhang F, Li C. Interface engineering of a CoO_x/Ta_3N_5 photocatalyst for unprecedented water oxidation performance under visible-light-irradiation. Angew Chem Int Ed 2015;54(10):3047–51.
[46] Kasahara A, Nukumizu K, Hitoki G, Takata T, Kondo JN, Hara M, et al. Photoreactions on $LaTiO_2N$ under visible light irradiation. J Phys Chem A 2002;106(29):6750–3.
[47] Hitoki G, Takata T, Kondo JN, Hara M, Kobayashi H, Domen K. An oxynitride, TaON, as an efficient water oxidation photocatalyst under visible light irradiation ($\lambda \leq 500$ nm). Chem Commun 2002;(16):1698–9.
[48] Hara M, Hitoki G, Takata T, Kondo JN, Kobayashi H, Domen K. TaON and Ta_3N_5 as new visible light driven photocatalysts. Catal Today 2003;78(1–4):555–60.
[49] Takata T, Pan C, Domen K. Design and development of oxynitride photocatalysts for overall water splitting under visible light irradiation. ChemElectroChem 2016;3(1):31–7.
[50] Matoba T, Maeda K, Domen K. Activation of $BaTaO_2N$ photocatalyst for enhanced non-sacrificial hydrogen evolution from water under visible light by forming a solid solution with $BaZrO_3$. Chemistry 2011;17(52):14731–5.
[51] Xu J, Pan C, Takata T, Domen K. Photocatalytic overall water splitting on the perovskite-type transition metal oxynitride $CaTaO_2N$ under visible light irradiation. Chem Commun 2015;51(33):7191–4.
[52] Maeda K. (Oxy)nitrides with d^0-electronic configuration as photocatalysts and photoanodes that operate under a wide range of visible light for overall water splitting. Phys Chem Chem Phys 2013;15(26):10537–48.
[53] He Y, Thorne JE, Wu CH, Ma P, Du C, Dong Q, et al. What limits the performance of Ta_3N_5 for solar water splitting? Chem 2016;1(4):640–55.
[54] Chun WJ, Ishikawa A, Fujisawa H, Takata T, Kondo JN, Hara M, et al. Conduction and valence band positions of Ta_2O_5, TaON, and Ta_3N_5 by UPS and electrochemical methods. J Phys Chem B 2003;107(8):1798–803.
[55] Balaz S, Porter SH, Woodward PM, Brillson LJ. Electronic structure of tantalum oxynitride perovskite photocatalysts. Chem Mater 2013;25(16):3337–43.
[56] Higashi M, Domen K, Abe R. Fabrication of efficient TaON and Ta_3N_5 photoanodes for water splitting under visible light irradiation. Energy Environ Sci 2011;4(10):4138–47.
[57] Yokoyama D, Hashiguchi H, Maeda K, Minegishi T, Takata T, Abe R, et al. Ta_3N_5 photoanodes for water splitting prepared by sputtering. Thin Solid Films 2011;519(7):2087–92.
[58] Feng X, Latempa TJ, Basham JI, Mor GK, Varghese OK, Grimes CA. Ta_3N_5 nanotube arrays for visible light water photoelectrolysis. Nano Lett 2010;10(3):948–52.
[59] Ritala M, Kalsi P, Riihelä D, Kukli K, Leskelä M, Jokinen J. Controlled growth of TaN, Ta_3N_5, and TaO_xN_y thin films by atomic layer deposition. Chem Mater 1999;11(7):1712–8.
[60] Fang Z, Aspinall HC, Odedra R, Potter RJ. Atomic layer deposition of TaN and Ta_3N_5 using pentakis(dimethylamino)tantalum and either ammonia or monomethylhydrazine. J Cryst Growth 2011;331(1):33–9.
[61] Zhen C, Wang L, Liu G, Lu GQ, Cheng HM. Template-free synthesis of Ta_3N_5 nanorod arrays for efficient photoelectrochemical water splitting. Chem Commun 2013;49(29):3019–21.
[62] Pinaud BA, Vailionis A, Jaramillo TF. Controlling the structural and optical properties of Ta_3N_5 films through nitridation temperature and the nature of the Ta metal. Chem Mater 2014;26(4):1576–82.
[63] Park JC, Pee JH, Park HH. Effect of presynthesis of Ta precursor on the formation of Ta nitrides. J Mater Res 2010;25(5):835–41.
[64] Kishida K, Watanabe T. Improvement of photocatalytic activity of tantalum nitride by ammonothermal treatment at high pressure. J Solid State Chem 2012;191:15–8.
[65] Lee Y, Nukumizu K, Watanabe T, Takata T, Hara M, Yoshimura M, et al. Effect of 10 MPa ammonia treatment on the activity of visible light responsive Ta_3N_5 photocatalyst. Chem Lett 2006;35(4):352–3.
[66] Brauer G, Weidlein JR. Synthesis and properties of red tantalum nitride Ta_3N_5. Angew Chem 1965;77(5):218–9. German.
[67] Murakami N, Prieto Mahaney OO, Abe R, Torimoto T, Ohtani B. Double-beam photoacoustic spectroscopic studies on transient absorption of titanium (IV) oxide photocatalyst powders. J Phys Chem C 2007;111(32):11927–35.
[68] Abe R, Takami H, Murakami N, Ohtani B. Pristine simple oxides as visible light driven photocatalysts: Highly efficient decomposition of organic compounds over platinum-loaded tungsten oxide. J Am Soc Chem 2008;130(25):7780–1.
[69] Takata T, Lu D, Domen K. Synthesis of structurally defined Ta_3N_5 particles by flux-assisted nitridation. Cryst Growth Des 2011;11(1):33–8.
[70] Xiao M, Li Y, Lu Y, Ye Z. Synthesis of ZrO_2: Fe nanostructures with visible-light driven H_2 evolution activity. J Mater Chem A 2015;3(6):2701–6.
[71] Li Y, Li F, Li X, Song H, Lou Z, Ye Z, et al. Ultrahigh efficient water oxidation under visible light: Using Fe dopants to integrate nanostructure and cocatalyst in $LaTiO_2N$ system. Nano Energy 2016;19:437–45.
[72] Shen S, Zhao L, Zhou Z, Guo L. Enhanced photocatalytic hydrogen evolution over Cu-doped $ZnIn_2S_4$ under visible light irradiation. J Phys Chem C 2008;112(41):16148–55.
[73] Hong J, Xia X, Wang Y, Xu R. Mesoporous carbon nitride with *in situ* sulfur doping for enhanced photocatalytic hydrogen evolution from water under visible light. J Mater Chem 2012;22(30):15006–12.
[74] Zuo F, Wang L, Wu T, Zhang Z, Borchardt D, Feng P. Self-doped Ti^{3+} enhanced photocatalyst for hydrogen production under visible light. J Am Chem Soc 2010;132(34):11856–7.
[75] Li Y, Ma G, Peng S, Lu G, Li S. Boron and nitrogen co-doped titania with enhanced visible-light photocatalytic activity for hydrogen evolution. Appl Surf Sci 2008;254(21):6831–6.
[76] Kado Y, Hahn R, Lee CY, Schmuki P. Strongly enhanced photocurrent response for Na doped Ta_3N_5-nano porous structure. Electrochem Commun 2012;17:67–70.
[77] Feng J, Cao D, Wang Z, Luo W, Wang J, Li Z, et al. Ge-mediated modification in Ta_3N_5 photoelectrodes with enhanced charge transport for solar water splitting. Chemistry 2014;20(49):16384–90.
[78] Ma SSK, Hisatomi T, Maeda K, Moriya Y, Domen K. Enhanced water oxidation on Ta_3N_5 photocatalysts by modification with alkaline metal salts. J Am Chem Soc 2012;134(49):19993–6.
[79] Xie Y, Wang Y, Chen Z, Xu X. Role of oxygen defects on the photocatalytic properties of Mg-doped mesoporous Ta_3N_5. ChemSusChem 2016;9(12):1403–12.
[80] Kado Y, Lee CY, Lee K, Müller J, Moll M, Spiecker E, et al. Enhanced water splitting activity of M-doped Ta_3N_5 (M = Na, K, Rb, Cs). Chem Commun 2012;48(69):8685–7.
[81] Seo J, Takata T, Nakabayashi M, Hisatomi T, Shibata N, Minegishi T, et al. Mg-Zr cosubstituted Ta_3N_5 photoanode for lower-onset-potential solar-driven photoelectrochemical water splitting. J Am Chem Soc 2015;137(40):12780–3.
[82] Pan C, Takata T, Kumamoto K, Khine Ma SS, Ueda K, Minegishi T, et al. Band engineering of perovskite-type transition metal oxynitrides for photocatalytic overall water splitting. J Mater Chem A 2016;4(12):4544–52.
[83] Xiong J, Han C, Li Z, Dou S. Effects of nanostructure on clean energy: Big solutions gained from small features. Sci Bull 2015;60(24):2083–90.
[84] Hisatomi T, Otani M, Nakajima K, Teramura K, Kako Y, Lu D, et al. Preparation of crystallized mesoporous Ta_3N_5 assisted by chemical vapor deposition of tetramethyl orthosilicate. Chem Mater 2010;22(13):3854–61.
[85] Maeda K, Nishimura N, Domen K. A precursor route to prepare tantalum (V) nitride nanoparticles with enhanced photocatalytic activity for hydrogen evolution under visible light. Appl Catal A Gen 2009;370(1–2):88–92.
[86] Yuliati L, Yang JH, Wang X, Maeda K, Takata T, Antonietti M, et al. Highly active tantalum (V) nitride nanoparticles prepared from a mesoporous carbon nitride template for photocatalytic hydrogen evolution under visible light irradiation. J Mater Chem 2010;20(21):4295–8.
[87] Tsang MY, Pridmore NE, Gillie LJ, Chou YH, Brydson R, Douthwaite RE. Enhanced photocatalytic hydrogen generation using polymorphic macroporous TaON. Adv Mater 2012;24(25):3406–9.
[88] John S. Strong localization of photons in certain disordered dielectric superlattices. Phys Rev Lett 1987;58(23):2486–9.
[89] Chen JIL, von Freymann G, Choi SY, Kitaev V, Ozin GA. Amplified Photochemistry with slow photons. Adv Mater 2006;18(14):1915–9.
[90] Wang Z, Hou J, Yang C, Jiao S, Huang K, Zhu H. Hierarchical metastable γ-TaON hollow structures for efficient visible-light water splitting. Energy Environ Sci 2013;6(7):2134–44.
[91] Fukasawa Y, Takanabe K, Shimojima A, Antonietti M, Domen K, Okubo T. Synthesis of ordered porous graphitic-C_3N_4 and regularly arranged Ta_3N_5 nanoparticles by using self-assembled silica nanospheres as a primary template. Chem Asian J 2011;6(1):103–9.
[92] Fu J, Skrabalak SE. Aerosol synthesis of shape-controlled template particles: A route to Ta_3N_5 nanoplates and octahedra as photocatalysts. J Mater Chem A 2016;4(21):8451–7.
[93] Maeda K, Terashima H, Kase K, Higashi M, Tabata M, Domen K. Surface modification of TaON with monoclinic ZrO_2 to produce a composite photocatalyst with enhanced hydrogen evolution activity under visible light. Bull Chem Soc Jpn 2008;81(8):927–37.
[94] Maeda K, Higashi M, Lu D, Abe R, Domen K. Efficient nonsacrificial water splitting through two-step photoexcitation by visible light using a modified oxynitride as a hydrogen evolution photocatalyst. J Am Chem Soc 2010;132(16):5858–68.
[95] Ma SSK, Maeda K, Domen K. Modification of TaON with ZrO_2 to improve photocatalytic hydrogen evolution activity under visible light: Influence of preparation conditions on activity. Catal Sci Technol 2012;2(4):818–23.
[96] Yuliati L, Maeda K, Takata T, Domen K. Modification of tantalum (V) nitride with zirconium oxide for photocatalytic hydrogen production under visible light irradiation. In: Proceedings of the 2012 International Conference on Enabling Science and Nanotechnology; 2012 Jan 5–7; Johor Bahru, Malaysia. Piscataway: IEEE; 2012. p. 1–2.
[97] Chen S, Qi Y, Ding Q, Li Z, Cui J, Zhang F, et al. Magnesia interface nanolayer modification of Pt/Ta_3N_5 for promoted photocatalytic hydrogen production under visible light irradiation. J Catal 2016;339:77–83.
[98] Qi Y, Chen S, Li M, Ding Q, Li Z, Cui J, et al. Achievement of visible-light-driven Z-scheme overall water splitting using barium-modified Ta_3N_5 as a H_2-evolving photocatalyst. Chem Sci 2017;8(1):437–43.
[99] Li R, Han H, Zhang F, Wang D, Li C. Highly efficient photocatalysts constructed by rational assembly of dual-cocatalysts separately on different facets of $BiVO_4$. Energy Environ Sci 2014;7(4):1369–76.
[100] Ma Y, Chong R, Zhang F, Xu Q, Shen S, Han H, et al. Synergetic effect of dual cocatalysts in photocatalytic H_2 production on $Pd\text{-}IrO_x/TiO_2$: A new insight into dual cocatalyst location. Phys Chem Chem Phys 2014;16(33):17734–42.
[101] Jiang Q, Li L, Bi J, Liang S, Liu M. Design and synthesis of TiO_2 hollow spheres with spatially separated dual cocatalysts for efficient photocatalytic hydrogen production. Nanomaterials 2017;7(2):24.
[102] Huang L, Wang X, Yang J, Liu G, Han J, Li C. Dual cocatalysts loaded type I CdS/ZnS core/shell nanocrystals as effective and stable photocatalysts for H_2

evolution. J Phys Chem C 2013;117(22):11584–91.
[103] Chang K, Mei Z, Wang T, Kang Q, Ouyang S, Ye J. MoS_2/graphene cocatalyst for efficient photocatalytic H_2 evolution under visible light irradiation. ACS Nano 2014;8(7):7078–87.
[104] Bi W, Li X, Zhang L, Jin T, Zhang L, Zhang Q, et al. Molecular co-catalyst accelerating hole transfer for enhanced photocatalytic H_2 evolution. Nat Commun 2015;6:8647.
[105] Yang J, Wang D, Han H, Li C. Roles of cocatalysts in photocatalysis and photoelectrocatalysis. Acc Chem Res 2013;46(8):1900–9.
[106] Maeda K, Abe R, Domen K. Role and function of ruthenium species as promoters with TaON-based photocatalysts for oxygen evolution in two-step water splitting under visible light. J Phys Chem C 2011;115(7):3057–64.
[107] Maeda K, Teramura K, Lu D, Saito N, Inoue Y, Domen K. Noble-metal/Cr_2O_3 core/shell nanoparticles as a cocatalyst for photocatalytic overall water splitting. Angew Chem Int Ed 2006;118(46):7970–3.
[108] Maeda K, Teramura K, Lu D, Saito N, Inoue Y, Domen K. Roles of Rh/Cr_2O_3 (core/shell) nanoparticles photodeposited on visible-light-responsive $(Ga_{1-x}Zn_x)(N_{1-x}O_x)$ solid solutions in photocatalytic overall water splitting. J Phys Chem C 2007;111(20):7554–60.
[109] Maeda K, Sakamoto N, Ikeda T, Ohtsuka H, Xiong A, Lu D, et al. Preparation of core-shell-structured nanoparticles (with a noble-metal or metal oxide core and a chromia shell) and their application in water splitting by means of visible light. Chemistry 2010;16(26):7750–9.
[110] Yoshida M, Takanabe K, Maeda K, Ishikawa A, Kubota J, Sakata Y, et al. Role and function of noble-metal/Cr-layer core/shell structure cocatalysts for photocatalytic overall water splitting studied by model electrodes. J Phys Chem C 2009;113(23):10151–7.
[111] Yagi M, Tomita E, Kuwabara T. Remarkably high activity of electrodeposited IrO_2 film for electrocatalytic water oxidation. J Electroanal Chem 2005;579(1):83–8.
[112] Zhao Y, Hernandez-Pagan EA, Vargas-Barbosa NM, Dysart JL, Mallouk TE. A high yield synthesis of ligand-free iridium oxide nanoparticles with high electrocatalytic activity. J Phys Chem Lett 2011;2(5):402–6.
[113] Nakagawa T, Bjorge NS, Murray RW. Electrogenerated IrO_x nanoparticles as dissolved redox catalysts for water oxidation. J Am Chem Soc 2009;131(43):15578–9.
[114] Yang L, Luo S, Li Y, Xiao Y, Kang Q, Cai Q. High efficient photocatalytic degradation of *p*-nitrophenol on a unique Cu_2O/TiO_2 p-n heterojunction network catalyst. Environ Sci Technol 2010;44(19):7641–6.
[115] Bessekhouad Y, Robert D, Weber JV. Photocatalytic activity of Cu_2O/TiO_2, Bi_2O_3/TiO_2 and $ZnMn_2O_4/TiO_2$ heterojunctions. Catal Today 2005;101(3–4):315–21.
[116] Daskalaki VM, Antoniadou M, Li Puma G, Kondarides DI, Lianos P. Solar light-responsive Pt/CdS/TiO_2 photocatalysts for hydrogen production and simultaneous degradation of inorganic or organic sacrificial agents in wastewater. Environ Sci Technol 2010;44(19):7200–5.
[117] Zhang LJ, Li S, Liu BK, Wang DJ, Xie TF. Highly efficient CdS/WO_3 photocatalysts: Z-scheme photocatalytic mechanism for their enhanced photocatalytic H_2 evolution under visible light. ACS Catal 2014;4(10):3724–9.
[118] Liu X, Zhao L, Domen K, Takanabe K. Photocatalytic hydrogen production using visible-light-responsive Ta_3N_5 photocatalyst supported on monodisperse spherical SiO_2 particulates. Mater Res Bull 2014;49:58–65.
[119] Luo Y, Liu X, Tang X, Luo Y, Zeng Q, Deng X, et al. Gold nanoparticles embedded in Ta_2O_5/Ta_3N_5 as active visible-light plasmonic photocatalysts for solar hydrogen evolution. J Mater Chem A 2014;2(36):14927–39.
[120] Jang JS, Kim HG, Joshi UA, Jang JW, Lee JS. Fabrication of CdS nanowires decorated with TiO_2 nanoparticles for photocatalytic hydrogen production under visible light irradiation. Int J Hydrogen Energy 2008;33(21):5975–80.
[121] Adhikari SP, Hood ZD, More KL, Ivanov I, Zhang L, Gross M, et al. Visible light assisted photocatalytic hydrogen generation by Ta_2O_5/Bi_2O_3, TaON/Bi_2O_3, and Ta_3N_5/Bi_2O_3 composites. RSC Advances 2015;5(68):54998–5005.
[122] Higashi M, Abe R, Ishikawa A, Takata T, Ohtani B, Domen K. Z-scheme overall water splitting on modified-TaON photocatalysts under visible light (λ < 500 nm). Chem Lett 2008;37(2):138–9.
[123] Tabata M, Maeda K, Higashi M, Lu D, Takata T, Abe R, et al. Modified Ta_3N_5 powder as a photocatalyst for O_2 evolution in a two-step water splitting system with an iodate/iodide shuttle redox mediator under visible light. Langmuir 2010;26(12):9161–5.